

## Koala 3D: A continuous climbing 3D printer

Maximiliano Vélez<sup>a</sup>, Efrén Toala<sup>a</sup>, Juan Cristóbal Zagal<sup>a,b,\*</sup>

<sup>a</sup> Department of Mechanical Engineering, University of Chile, Santiago 8370448, Chile

<sup>b</sup> Millennium Nucleus on Soft Smart Mechanical Metamaterials, Santiago, Chile

### ARTICLE INFO

#### Keywords:

Construction 3D printing  
Climbing robot  
Free form fabrication  
Climbing 3D printer

### ABSTRACT

The size of manufactured parts is naturally bound by the size of their production machines. In this paper, we explore the alternative of making a machine that can continuously navigate along an object being fabricated, producing objects larger than itself. The machine combines a climbing robot and a 3D printer. It uses an infinite fabrication loop which includes printing, reanchoring to a new station, and printing again. We present the design, construction, and characterization of the machine along with experiments on the fabrication of vertical columns. We also demonstrate the freeform fabrication capabilities of the machine by printing a moai statue. The results obtained have a wide range of applications for construction, product fabrication and promisingly broaden the current applications of 3D printing.

### 1. Introduction

Manufacturing machines are usually capable of making parts that are smaller than production machines themselves [1]. For example, while a plastic injection molding machine usually occupies various cubic meters, it produces parts that are considerably smaller than itself, somewhere between several cubic centimeters. Similar situations arise with subtractive manufacturing machines, such as mills, lathes, and their CNC counterparts.

Additive manufacturing machines show a different trend, particularly observed among desktop 3D printers [2–4]. While the machine volume is still larger than the volume of produced parts the ratio of machine volume vs the volume of the produced part is closer to one.

In 2013 Lipson and Kurman [5] summarized ten underlying principles of 3D printing. In their seventh principle—of compact portable manufacturing—they remarked upon the enormous per volume production capacity of 3D printers because these machines produce objects as large as their printing volume, which is not substantially smaller than the volume of the complete machine. Also they explain that the potential of 3D printers to enable compact, portable manufacturing is closely related to a transition from current centralized mass manufacturing [6] to distributed cloud manufacturing [7] in the future. They envisioned an interesting hypothetical case to elaborate on this, “If a 3D printer is arranged so its printing apparatus can move freely, a 3D printer can fabricate objects larger than itself” [5].

Developing manufacturing machines with the capability to produce objects larger than themselves will open many possibilities for the

progress of the construction industry [8] and product development [9]. Larger objects and buildings are usually manufactured by aggregating interlocked components. Interestingly, 3D printing has already demonstrated the capacity to directly produce interlocked components without assembly lines [5]. Scaffolding, human assistance, and heavy machinery is usually required for stacking construction material or carrying it to the top of a structure being built. The alternative of using autonomous machines that can navigate and carry material along structures that are being fabricated is promising.

This paper explores the alternative of producing a machine (a combination of a robot and a 3D printer) capable of producing structures larger than itself by navigating vertically along the object being built. Noticeably, it is the machine that moves along the object and not an object emerging from a static platform. The paper is divided into 6 sections. Section 2 provides background on the work related to the proposed task. Section 3 presents the conceptual design of the machine. Section 4 elaborates on the design and construction of the 3D printer. Section 5 explains a series of experiments and performance evaluations. Section 6 provides a discussion about the work. Finally, Section 7 concludes the paper and offers the future applications of the study.

### 2. Related work

The machine presented in this work is inspired in ideas and technologies from at least five different research topics, which are (1) additive manufacturing, (2) large scale additive manufacturing, (3) autonomous collaborative robotic assembly, (4) vertical slipform

\* Corresponding author at: Department of Mechanical Engineering, University of Chile, Santiago 8370448, Chile.

E-mail address: [jczagal@ing.uchile.cl](mailto:jczagal@ing.uchile.cl) (J.C. Zagal).

<https://doi.org/10.1016/j.rcim.2020.101950>

Received 24 March 2019; Received in revised form 17 December 2019; Accepted 19 January 2020

Available online 10 March 2020

0736-5845/ © 2020 Elsevier Ltd. All rights reserved.

**Table 1** Summary of machines that can fabricate structures larger than themselves. Maximum building dimensions are given in either Cartesian (x,y,z) or cylindrical (r,θ,z) coordinates.

| Device name                              | Developer                       | Technology   | Building material           | Building speed                       | Volume / weight ( $m \times m \times m$ / kg) | Maximum building dimension (m)   |
|--|---------------------------------|--|-----------------------------|--------------------------------------|---|----------------------------------|
| DCP                                      | Keating et al. [19]             | Robocasting  | Polyurethane                | 0.5 m / s                            | $4 \times 5 \times 10$ / 6350                 | $4.0z \times 10.0r$              |
| Minibuilders                             | IACC [21]                       | Robocasting  | Concrete                    | $0.03 \text{ m}^3$ / h               | $0.27 \times 0.35 \times 0.32$ / 10           | 3.0z                             |
| Fiberbot                                 | Kayser et al. [22]              | Robocasting  | Fiber / Resin               | 0.8 m / h                            | $0.3 \times 0.3 \times 0.5$ / 0.5             | 4.5z                             |
| Blackbelt 3D printer                     | Blackbelt 3D printer<br>BV [23] | FDM  | ABS / PLA / Copolyester     | $24 \text{ mm}^3$ / s                | $0.4 \times 0.45 \times 0.8$ / 1.0            | $0.34x \times 1.3y \times 0.34z$ |
| Aerial 3D printer                        | Hunt et al. [24]                | Robocasting  | Polyurethane                | 10 ml / 200s                         | $0.3 \times 0.47 \times 0.7$ / 1.3            | 1.0r                             |
| Termites-based robot                     | Werfel et al. [25]              | Autonomous collaborative robotic construction by stacking bricks     | Urethane blocks             | 3 robots stacking 4 bricks in 23 min | $0.11 \times 0.175 \times 0.195$ / 0.8        | 0.225z                           |
| Block manipulator quadcopter             | Willmann et al. [27]            | Autonomous collaborative robotic construction by stacking bricks     | Polyurethane foam blocks    | 1500 foam blocks in 18 h             | $0.54 \times 0.54 \times 0.85$ / 0.7          | $9.0x \times 9.0y \times 9.0z$   |
| Cable bridge fabricated by flying robots | Mirjan et al. [28]              | Autonomous collaborative robotic construction by tensile aggregation | Polyethylene rope (Dyneema) | 75 m / s                             | $7.5 \times 0.6 \times 0.7$ / 0.4             | 7.5x                             |

construction and (5) truss forming machines for space applications. In this section we review the recent research on these areas.

### 2.1. Additive manufacturing

Additive manufacturing (3D printing) is today a rapidly growing area of research. It's potential for freeform fabrication of complex parts, mass customization, waste minimization and zero lead time production makes 3D printing applications to flourish in a variety of fields [10]. Research topics include the development of new 3D printing materials, methods and applications. New materials include ceramics, smart materials, biomimetic materials [11] and biocompatible composites [12]. Development of new methods is often concentrated on improving fabrication speed [13], reducing material waste [14,15], increasing printing resolution, exploring the use of different materials [16] and expanding the range of scales at which 3D printing is possible.

### 2.2. Large scale additive manufacturing

Table 1 summarizes developments and research related to the present work. In the first group of additive manufacturing machines we mention the recent work on self-sufficient robotic fabrication at architectural scales by Keating and colleagues [19]. They demonstrate the possibility of mounting a large material extruder on top of a tracked mobile robot with their Digital Construction Platform (DCP). The platform can horizontally commute between different locations. Once fixed in a place, a robotic arm is responsible for executing volumetric extrusion paths. As a result, the platform can produce structures that are 3.7 m tall. This height is limited by the length of the arm itself.

A similar result was recently obtained by a team of collaborating robots [20]. While not academically published, the work on Mini-builders [21] conducted at IACC Barcelona is an interesting advancement in moving extrusion tools along the geometries being built. However, these extrusion tools are limited to following or repeating pre-established paths, which limits their application to some fixed form tasks. Similarly Fiberbots [22] is a robot capable of winding fiber and resin cylindrically around itself producing vertical tubes.

Another interesting development is the Blackbelt [23] Y-unlimited 3D printer. While the printer is static, it has a conveyor belt mounted on its printing platform. The machine can produce parts that are unlimited along the Y-axis because the belt is free to move along the Y-axis. The possibility of truly xyz-unlimited 3D printing has been explored with flying robots [24]. However, these machines have not demonstrated the capability to fabricate complex forms yet. Instead, the current work is limited to repair of failures at coarser levels of detail.

### 2.3. Autonomous collaborative robotic assembly

Various robotic systems [13] with the capability to assemble structures from building blocks have been proposed. Perhaps one of the most notable examples is the work on termite-inspired decentralized construction robots [25]. These robots can stack bricks and assemble complex structures following principles of stigmergy [26]. These robots can also navigate along the structures being built. The largest structure constructed by a group of collaborating robots was produced by flying stacking robots in the work of Willmann and colleagues [27]. A  $9 \times 9 \times 9$  m brick-based structure was generated in their study. The trajectories of the flying robots were commanded using a centralized system and a global motion capture system. In this case the main spatial limitation is the volume that the motion capture system can accurately cover. Mirjan et al. [28] demonstrated the possibility of building a 7.5 m length cable bridge with a set of cooperating autonomous flying machines. The process required flying robots to braid the primary elements of the structure by themselves.

#### 2.4. Vertical slipform construction

The principle of reanchoring a manufacturing platform to different stations while fabricating a vertical structure has been used in civil engineering. Vertical slip forming [29] used to produce large concrete structures such as silos, towers and dams is one such case. An initial form is surrounded by a platform on which workers pour concrete and place reinforcing metal rods. Once the concrete hardens, the platform is raised by hydraulic jacks to a new station repeating the process. The limited form variability during construction is one of the main drawbacks of the process. Another example is the tower cranes that are also anchored to different vertical stations while subsequent components are lifted while constructing a building. However, these examples are still far from being automated. Cranes and hydraulic jacks are always controlled by human operators and workers must take on multiple manual operations for these processes to occur.

#### 2.5. Truss forming machines for space applications

The technical feasibility of in-space automated construction of large truss-based structures such as antennas, solar arrays, and optical systems have been studied by the NASA funded SpiderFab and Trusselator projects [17,18]. One interesting result is Trusselator, an automated truss forming machine. This device continuously interweaves metal wires giving rise to truss structures. Experiments on earth keep the machine static on the ground while a continuous truss emerges vertically. The machine is expected to operate in space where the absence of gravity should enable the Trusselator to navigate along the generated trusses. However, this capability has not been demonstrated yet.

### 3. Conceptual design of Koala 3D

Initially the design of the printer was conceptualized by defining two critical components for its functioning. The first is a printer header part (See Fig. 1 inlet in cyan) that should always be on top of the fabricated beam. The second is the climbing part (Fig. 1, inlet in green) that keeps the first part in position. The climbing part was expected to be implemented with a pair of robotically actuated clamps. A Lower Clamping Mechanism was located at the bottom of the printer body while an Upper Clamping Mechanism was free to move between the bottom and upper part of the printer. The idea is to convert this limited range of motion into an infinite range by changing the anchoring points, always having one clamp attached to the beam. Fig. 1, right, illustrates the phases of the motion consisting of a printing phase, during which the upper clamp is secured allowing the slow vertical motion of the printer relative to it and a reanchoring stage, during which the lower clamp temporarily secures the printer to the beam while the upper clamp releases itself and transitions to the upper limit of the vertical rail travel to find its new anchoring point. As Fig. 1 indicates, this repeated process of printing-reanchoring-printing-reanchoring can be executed constantly until a desired beam height is obtained.

### 4. Desing of the working prototype

The printer can be decomposed into two major subsystems. One is the vertical climbing stage for reanchoring, precise vertical motion during printing, as well as carrying the electronics. The other subsystem is the x-y positioning stage for moving the printer extruder. This stage also carries the material impulsion system.

Fig. 2 shows the main components of the final design of Koala 3D printer. A base plate (a) supports the y-rack, y-rails and the y-endstop switch. The y-carriage (b) supports the y-motor, the x-rack, the x-rails and the x-endstop. The x-carriage (c) supports the x-motor and the extruder. Servo base plates (d) are secured to the lower and central carriages of the climbing part. Each servo subassembly drives a lead-screw that transmits force to the clamping carriage jaw (e). Two

retractile wheels allow guiding the vertical movement of the robot while also permit a secure clamp when retracted. The lower clamping carriage LCC hold a lifting motor and lead screw shown in (f). The central clamping carriage CCC (g) has a nut that joins to the lead screw from LCC. The upper carriage (h) is not motorized and has a counter-weight for displacing the center of mass. The following subsections describe the design of each subsystem.

#### 4.1. X-Y positioning stage

We chose to design a more robust positioning system that combines elements existing in popular 3D printers with some key improvements to reduce the size and weight of the positioning stage. The stage was designed to cover an extruder motion range of 45 mm x 45 mm on the x-y plane. We expected to produce vertical beams having a sectional area of 30 mm x 30 mm with this motion span. The extra motion span (50% larger on every dimension) was intended to allow the extruder to purge outside the printing area as well as potentially introduce some features on the surface of the produced beam.

It was observed that most x-y positioning stages used on 3D printers rely on motion belts driven by timing pulleys. The driving motor is often kept aside from the motion rails and one extra pulley is used to transmit power to the stage. The design was too voluminous for our purposes. Therefore, we opted to position the driving motors in the middle of the rails and transmitted power by means of pinion and rack mechanism. This also required fewer components.

Motors were selected based on their torque, speed, controllability, and cost. The maximum acceleration was estimated to take place when the printing heads transition from 0 mm/s to 0.1 mm/s in 0.1 s by observing the motion of most popular 3D printers [30,31]. This yields an acceleration in the range of  $\ddot{v} = 1 \text{ mm/s}^2$ . As shown in Fig. 2(b), the motor working the most should move the weight of the y-stage which simultaneously supports the x-stage and extruder. We rounded this weight to be  $m = 1 \text{ kg}$  from component specifications. Eq. (1) indicates that the required force  $F_{GY}$  was estimated to be in the range of  $F_{GY} = 1 \text{ N}$ .

$$F_{GY} = m\ddot{v} \quad (1)$$

The effective radius of each pinion exerting force on its rack was considered  $R_G = 2.3 \text{ cm}$ . To estimate the required motor torque  $T_{GY}$ , we replace  $R_G$  in Eq. (2) resulting in  $T_{GY} = 0.023 \text{ N}$ .

$$T_{GY} = R_G \times F_{GY} \quad (2)$$

Knowing these requirements, a Nema 16 stepper motor with  $T_{GY} = 0.17 \text{ Nm}$  at 12 V and 2 A was selected. Although this motor provides a much higher torque, it was commanded in 1/8 micro stepping mode, yielding higher torque requirements.

#### 4.2. Filament impulsion and printing head

A J-Head E3D extruder was selected for its compact design, reduced weight, and reported performance [32]. The material impulsion system was placed away from the x-y positioning stage and guided the filament through tubing considering the space limitations and to reduce the load on the motors. We used the freely available Bowden material impulsion design which is a material impulsion unit located apart from the printing head. The material is guided into the extruder using a plastic tube [33].

#### 4.3. Design of vertical climbing stage

The vertical climbing stage (VCS) is one of the most challenging components of the printer since it must allow the entire mechanism to climb along the vertical beam and it must do so in coordination with the printing process. Any misplacement of the printer from the vertical beam would cause errors in deposition of material layers and



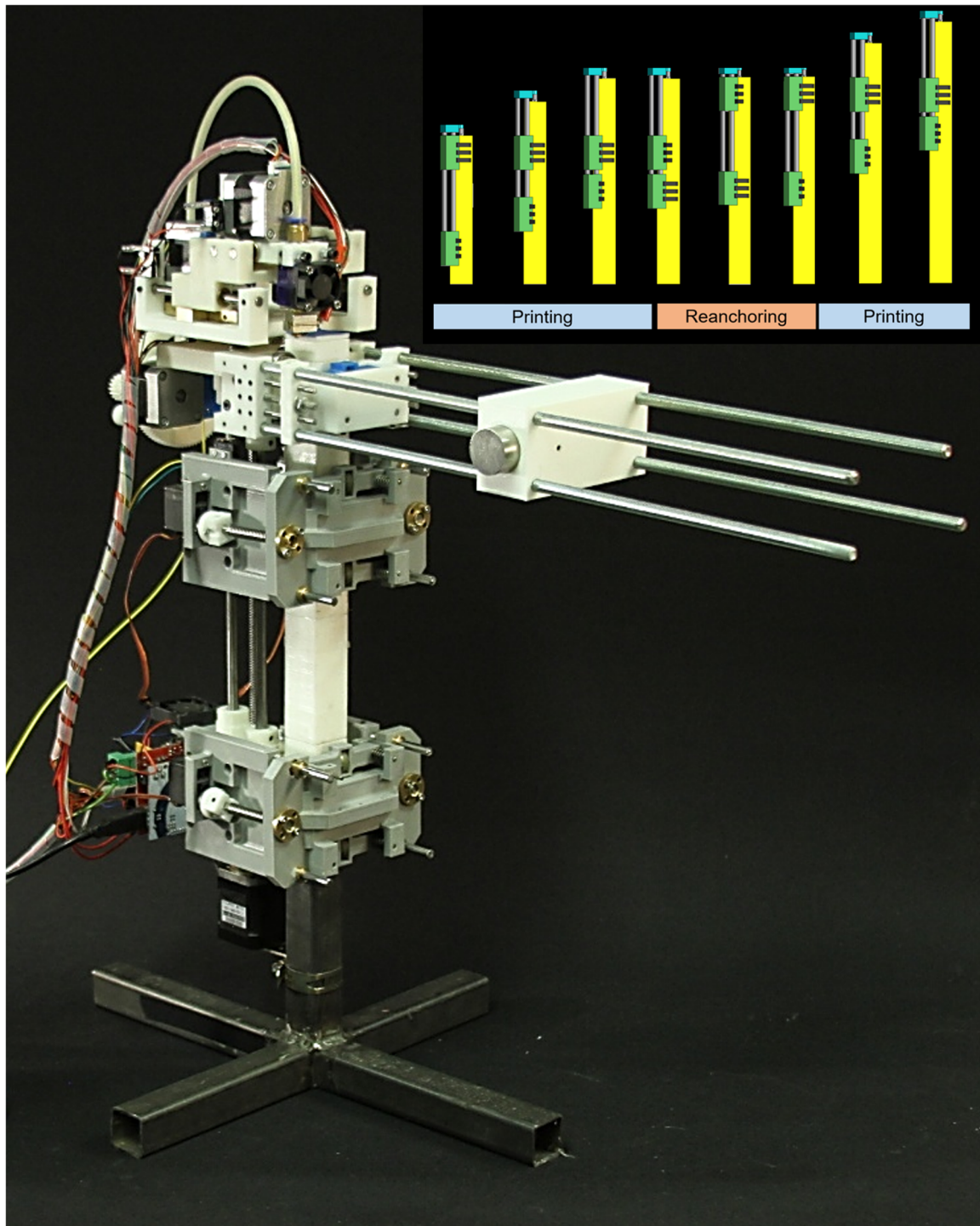


Fig. 1. Left: Koala 3D mounted on its printing base. Upper inlet: Printing and reanchoring phases of the fabrication process.

eventually, fail the entire fabrication process.

Traditional 3D printers can control the vertical position of printing heads with high precision usually by using leadscrews. An infinite vertical leadscrew would be an ideal solution for this machine. However, this is not realistic. The aim was to keep the machine size compact and independent of the structure being produced. Therefore, the selected alternative had to use a finite length leadscrew that could be anchored and translated when combined with a pair of clamping carriages.

A motorized central clamping carriage (CCC, see Fig. 2(g)) anchors the machine to the beam during printing, while a motorized leadscrew

(Fig. 2(f)) pulls the printer up relative to a threaded nut (Fig. 2(g)) placed at the CCC. Once the lower clamping carriage (LCC, Fig. 2(f)) reaches the CCC, reanchoring takes place. This phase anchors the LCC to the beam and releases the CCC (Fig. 2(g)). Once the CCC is free, it is translated into a new anchoring point by rotating the leadscrew in the opposite direction.

Fig. 2 details the CCC, LCC and UC components. Fig. 2(g) shows the position of the threaded nut and bushings that allow the CCC to slide along linear shafts. These elements are aligned with the LCC motorized leadscrew and the 8 mm linear shafts fixed to the LCC (Fig. 2(f)) respectively. The LCC also includes the z-stepper motor, the motor mount



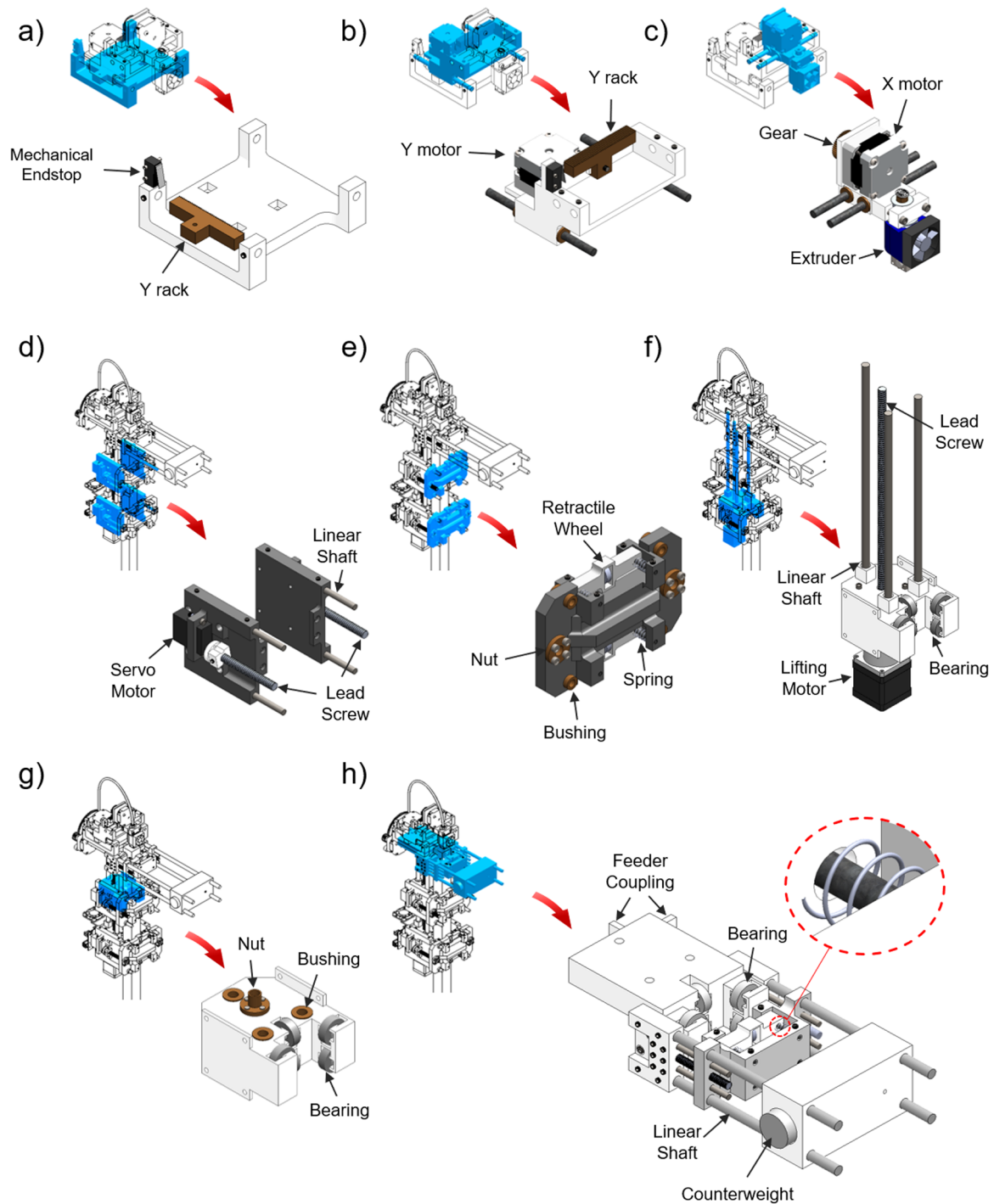


**Fig. 2.** Details of the final design of Koala 3D printer. The x-y extrusion positioning stage consists of a base plate (a), the y-carriage (b) and the x-carriage (c). Details of the clamping carriage are shown in (d) and (e). The lifting motor screw and central clamping carriage nut are shown in (f) and (g). The counter balance mechanism is shown in (h).

and motor coupler. Fig. 2(c) shows the UC that consists of bearings and a mounting plate above to support the x-y stage. It does not carry any lateral support surface. The position of rolling bearings, (six on each carriage core) that allow the carriage to slide along the beam, is also shown. A flat fixture plate left on each side of the clamping carries the motorized clamps.

Fig. 2(d), (e) shows the design of the LCC and CCC motorized jaws. Both carriages have identical jaws. Fig. 2(d) displays the position of the lateral fixtures that guide the motion of the jaws. Each fixture supports a pair of linear shafts and one servo motor driven leadscrew. Fig. 2(e)

shows the movable jaw that comprises two threaded nuts that align each with corresponding leadscrew and four bushings that align with the linear shafts. A retractile wheel mechanism is also part of this jaw. The retractile mechanism consists of two wheels mounted on sliding supports. These supports move along cylindrical shafts and can exert pressure against the beam due to the use of springs.

Fig. 2(e) shows the retractile wheel mechanism of the moving jaw. This mechanism was devised for the double function required for the clamping carriages. We observed that the sole contact between bearings and beam does not effectively clamp. Conversely, bearings are required

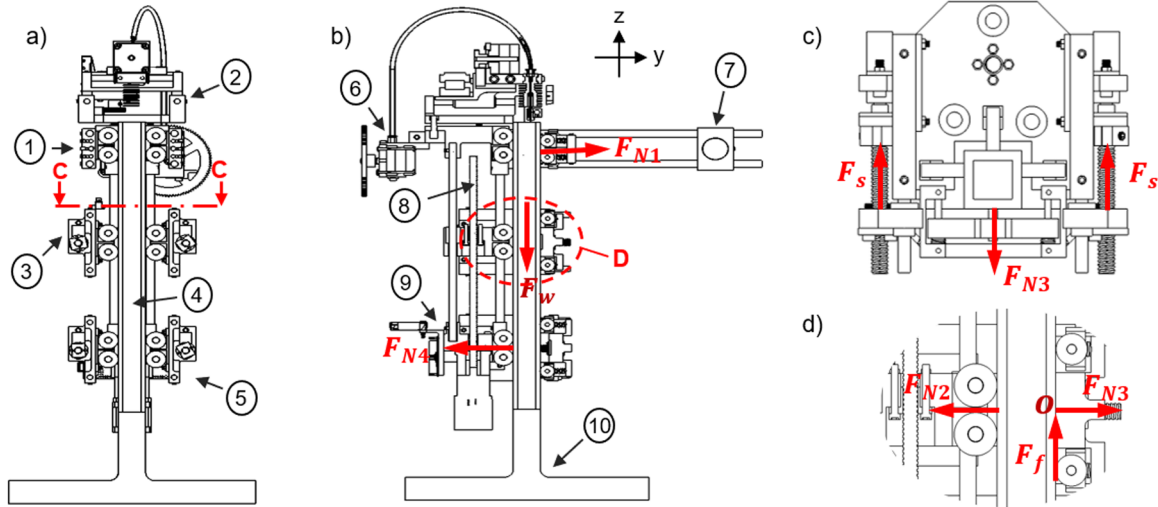


**Fig. 3.** (a) Longitudinal cut front view. 1 Upper carriage 2 x-y stage 3 Central carriage 4 Printed column 5 Lower clamping carriage (b) Free body diagram when Koala is in printing process. In this stage the central clamping carriage is holding the whole machine while the lower clamping carriage is guiding the movement through the column. 6 Material feeder 7 Counterweight 8 Leadscrew 9 Control board (c) C–C cut view. Free body diagram of central clamping press during the printing stage (d) D detail. Forces on CCC during the printing process.

for to allow motion during the vertical motion of the carriage. Therefore, we devised a mechanism that allows the bearings to retract while applying sufficient clamping pressure with the pair of motorized leadscrews, leaving a flat portion of the moving jaw to make full contact with the beam.

A static force analysis was used to select the springs required under the most demanding situation where the robot is only held by the CCC and vertically equilibrated by lateral forces exerted by the LCC and UCC. Fig. 3(b), (d) display red vectors representing the main forces considered in the analysis. Eq. (3) corresponds with the equilibrium of forces in the Y-axis with the normal forces ( $F_{Ni}$ , with  $i = \{1, \dots, 4\}$ ) acting over LCC, CCC, and UCC. Eq. (4) represents the equilibrium of forces in the Z axis considering the overall weight of the printer  $F_w$  acting over the center of mass and the friction force  $F_f$  while the CCC is anchored. Equilibrium of torques over the indicated “o” point (see Fig. 3(d) inlet) yields Eq. (5) where the torque distances of each normal force  $F_{Ni}$  pointing to “o” are noted by  $d_i$  and the distance to the center of the mass denoted by  $d_w$ .

$$\sum F_y = 0 \rightarrow F_{N1} - F_{N2} + F_{N3} - F_{N4} = 0 \quad (3)$$

$$\sum F_z = 0 \rightarrow -F_w + F_f = 0 \quad (4)$$

$$\sum M_o = 0 \rightarrow F_w d_w - (F_{N1} d_1 + F_{N4} d_4) = 0 \quad (5)$$

$$F_f = \mu F_{N3} \quad (6)$$

$$F_{N1} = 4 k x_1 \quad (7)$$

Eq. (6) notes the relation between friction  $F_f$  and  $F_{N3}$ . Eq. (7) represents the relation between normal force  $F_{N1}$  and the force resulting from four springs, with the same elastic constant  $k$ , displaced by a distance  $x_1$ .

The assumption that forces exerted by the CCC over the column are aligned yields to  $F_{N2}$  to be equal in modulus to  $F_{N3}$ . Applying this to Eq. (3) implies that  $F_{N1}$  and  $F_{N4}$  are also equal. The constant  $k$  of the springs can be derived by considering these relations and replacing them in Eq. (5) and in the expressions for  $F_f$ ,  $F_{N1}$  and  $F_{N3}$  described in Eqs. (4), (6) and (7). This requires the information about the printer weight (minus the weight of the CCC)  $F_w$ , shown in Table 2, the expected geometrical deformation of springs  $x_1$  (see Table 3), the friction coefficient existing between clamp and column (set to  $\mu = 0.3$ , from Gustafsson [34]), the distance from point O to the printer centroid

**Table 2**

Main characteristic of Koala 3D printer.

| General design                              |   |
|---|---|
| Extruder Type                               | E3D V6 1,75mm                             |
| 3D Printing material                        | PLA                                       |
| Cooling system                              | Air-cooled by fan                         |
| Z motion system                             | Power screw                               |
| X-Y platform system: Transmission system    | Gear-rack set Linear shaft                |
| Guiding system                              |   |
| Material feeder                             | Bowden extruder                           |
| Machine-Beam Support                        | Clamps                                    |
| Mechanism for modifying the center of mass. | Static Counterweight (600 grms)           |
| Physical characteristics                    |   |
| Work area x-y                               | $x = 47 \text{ mm}$ ; $y = 42 \text{ mm}$ |
| Z range                                     | Not restricted by design                  |
| Weight ( $F_w$ )                            | 7 Kg                                      |
| Control software                            |   |
| Control Board                               | Arduino Mega 2560 and Ramps 1.4           |
| Firmware                                    | Marlin                                    |
| Manufacturing details                       |   |
| Cost of the-shelf-parts                     | 271.19 USD                                |
| Cost of fabricated parts.                   | 878.11 USD                                |
| Time required for assembly.                 | 100 HH                                    |
| Time required for printing required parts.  | 113 Hrs.                                  |
| Performance (max/nominal)                   |   |
| z-axis feed speed.                          | 130 mm/s                                  |
| mm / per minute                             | 24 – 16                                   |
| x-y feed speed.                             | 60 mm/s – 50 mm/s                         |
| Max resolution in z                         | 0.10 mm / 0.30 mm                         |
| Rugosity in side of beam (RMS)              | 46.42 / 37.13                             |
| Power consumption                           | 50W                                       |

( $d_w = 15 \text{ mm}$ ), and the distance from point O to forces  $F_{N1}$  and  $F_{N4}$  ( $d_4 = d_1 = 137.5 \text{ mm}$ ).

Replacing all these values in Eq. (8) yields a spring constant  $k = 2071.26 \text{ N/m}$ . Finally, using the helical spring design in Eq. (9), and using Roslau wire defines the number  $N = 5$  of spring turns and the spring diameter  $D = 4 \text{ mm}$ . The four springs will lead to a force  $F_{N1} = 12.43 \text{ N}$  that holds the printer in place.

$$k = \frac{F_w d_w}{4\mu x_1 (d_1 + d_4)} \quad (8)$$

**Table 3**  
Main mechanical components and its characteristics.

|  |                        |
|--|------------------------|
| <b>Roslau Steel Spring</b>                       |                        |
| Location on Prototype                            | UC, CCC, LCC           |
| Shear Modulus (G)                                | 79 Gpa                 |
| Spring Diameter (D)                              | 4 mm                   |
| Wire Diameter (d)                                | 1 mm                   |
| Spring Deformation ( $x_1$ )                     | 1 mm                   |
| <b>304 Steel Power Screw</b>                     |                        |
| Location   | LCC                    |
| Screw Diameter                                   | 8 mm                   |
| Lead of Thread                                   | 8 mm                   |
| Thread Angle                                     | 29°                    |
| <b>Stepper Motor Nema 16</b>                     |                        |
| Location   | x-carriage, y-carriage |
| Step Angle                                       | 1.8°                   |
| Phases   | 2                      |
| Maximum Torque                                   | 0.18 N.m               |
| Weigth   | 0.2 kg                 |
| <b>Stepper Motor Nema 17 with Gear Reduction</b> |                        |
| Location   | LCC                    |
| Step Angle                                       | 1.8°                   |
| Phases   | 2                      |
| Maximum Torque                                   | 1.68 N.m               |
| Weigth   | 0.6 kg                 |
| Gear reduction                                   | 5:1                    |
| <b>Servo Motor (GS-3630BB)</b>                   |                        |
| Location   | CCC,LCC                |
| Maximum Torque                                   | 0.28 N.m               |
| Maximum Speed                                    | 300°/s                 |
| Weigth   | 37 g                   |

$$k = \frac{d^4 G}{8D^3 N} \quad (9)$$

#### 4.4. Selection of lifting motor

The lifting motor is attached to the LCC and drives a leadscrew. The leadscrew runs across a nut attached at the CCC. Initially, the motor torque was estimated from the power screw design equation [34] that relates the printer weight  $F_w$  to the torque required to hold the screw still and the geometric design of power screw (see 304 Steel Power Screw, on Table 3). This model yields the minimum torque required  $T = 0.16$  Nm to hold the printer in place. In practice, however, we found that a motor with much higher holding torque was required for it to perform well. This discrepancy between theory and practice is probably due to the use of microstepping [35] (at 1/16 rate) and the motion dynamics that are not considered in the static model. We finally chose to use a Nema 17 stepper motor combined with the specified gear reduction box to provide 1.68 Nm torque (see Table 3).

#### 4.5. Selection of clamping motors

We selected small servo motors for the clamping task because they are compact, light, and have high torque. Moreover, clamping did not demand precision. Its motion was commanded in an open loop, assigning a certain actuation period for clamping and another to release the operation.

Fig. 3(b) shows the location of the CCC (marked as “D”) and details the forces in c and d inlets. As described in Eq. (10), we established that the total friction force  $F_f$  caused by the clamping operation should at least be equal to the weight of the printer being supported  $F_w$ . Eqs. (11) and (12) relate the normal force  $F_n$  exerted by the clamp against the column with  $F_f$  and with the forces  $F_s$  exerted by each of the two small servo-motor-driven lead screws mounted on each clamp (see Fig. 2(d)). The force friction coefficient [36] was  $\mu = 0.3$ .

$$F_w = F_f \quad (10)$$

$$F_f = \mu \times F_n \quad (11)$$

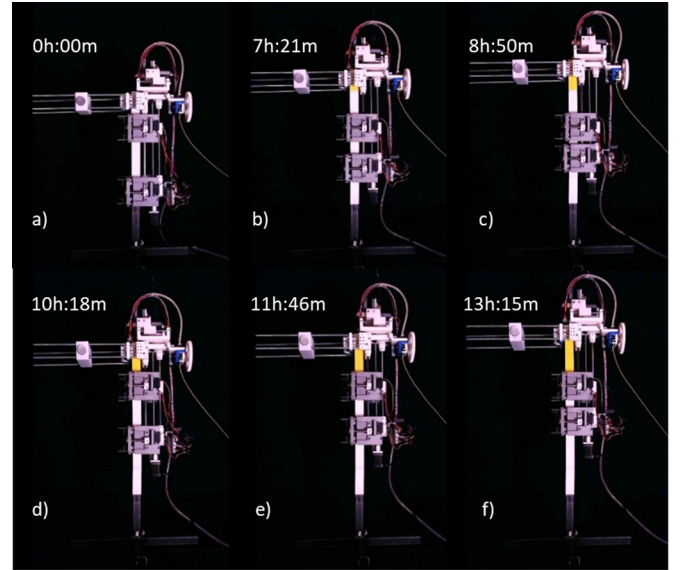


**Fig. 4.** Time-lapse of the printing process of a column 30 × 30 mm section and 200 mm high. (a)-(b) first printing phase; (c)-(d) reanchoring process; (e)-(f) second printing phase.

$$2 F_s = F_n \quad (12)$$

Replacing Eqs. (10) and (11) into (12) results in  $F_s = 114.4$  N.

The servo-motor-driven lead screws were selected to be of trapezoidal ACME type (details in Table 3). Each screw was transmitting force due to a nut mounted on the clamp as shown in Fig. 2(e). Using the same equations from previous section we established that the minimum torque required for each servo motor was 0.245 Nm. Table 3 also shows the details of the selected servo motor. Finally, this motor resulted in a servo motor sub assembly force of  $F_s = 137.23$  N.

## 5. Experiments and performance evaluation

### 5.1. Fabrication test

Fig. 4 shows the successful fabrication of a 200 mm height column (shown in yellow) at various time intervals. The fabrication process (shown in supporting video 1) took 13.25 h. The sequence identifies the initial printing (a-b), subsequent reanchoring (c-d), and final printing (e-f) stages for producing this part. Most time was spent in printing while it took only 1 min to execute the reanchoring stage, during which the printer accelerated to a vertical motion speed of 2 mm/s.

Resuming printing after reanchoring was a challenging problem. We found that the vertical position of the printer was affected after completing the reanchoring stage. Translating the machine weight from one anchoring point to another lead to a consistent drop of the entire mechanism. The limited rigidity of the structure was responsible for this displacement. We managed to reduce the displacement from 300 μm down to 60 μm by strengthening the design of clamping carriages (Fig. 7(a-c) shows the machine drop measuring procedure). The displacement problem was overcome with a motion command (simply G1 Z0.06 in machine code) that translated the machine 60 μm vertically before resuming printing to avoid adding extra weight required for further improving stiffness. This addressed the problem.

Fig. 5(c) shows an example (case 1, 15 mm height column) of initial, unsuccessful printing trials. The failure was caused by the horizontal displacement (see magnification on top inlet) of the new part with respect to the starting auxiliary platform (white). The displacement prevented the upper carriage from rolling across the interphase between the new material and auxiliary platform which, subsequently, blocked the entire mechanism.



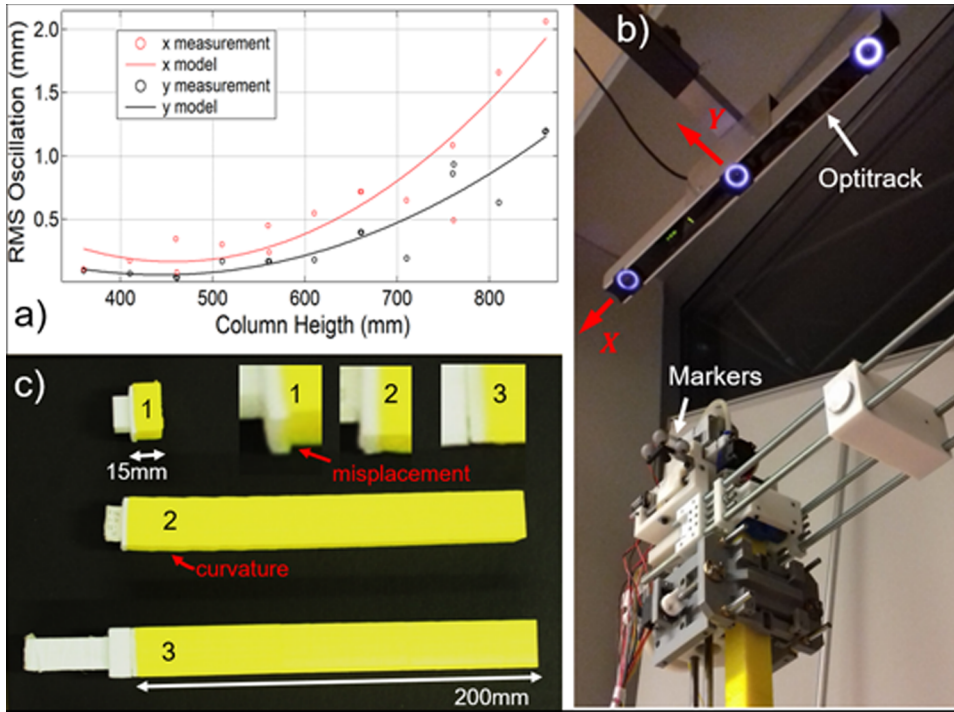


Fig. 5. (a) Root mean square of the x and y oscillations at different height during the printing process of a 400 mm beam; (b) Experimental setup used to measure the oscillations at the end of the column; (c) Samples test of the printing process of a 200 mm column. If the column was more aligned with the printing base, there would be less possibilities for failure in the printing process.

We obtained much larger parts (200 mm long) that initially exhibited a slight curvature along the vertical z-axis after reducing these displacement errors w. Fig. 5(c) illustrates an example of such a result (case 2). This curvature was attributed to initial lateral displacements. It can be seen that this initial curvature is self-corrected during the printing process (case 2-right hand side).

Finally, we obtained completely straight parts while eliminating the displacement. Fig. 5(c), case 3 illustrates this point. The magnification on the inlet shows that there is no mismatch between the white and yellow material.

We further investigated the capability of the printer to produce much larger parts. When printing at approximately 1 m on the beam, we observed that the constant motion of the printing head induced lateral oscillations on the resulting structure. It is natural to expect this effect on a thin beam supporting a moving heavy weight on top. Since this process might set a theoretical limit to the height of printed parts, we attempted to quantify its potential effect.

A set of eleven beams was fabricated as an initial auxiliary platform of varying between 350 mm to 850 mm high. We printed an additional, small part using the Koala 3D printer while simultaneously recording the lateral oscillation at the top of the printer for each platform. An Optitrack [37] optical motion capture system was used with spherical markers mounted atop the structure. Fig. 5(b) displays the position of Optitrack with respect to the printer, the orientation of the measuring coordinate system as well as the markers location (Supporting video 3 shows the printing process).

We collected position data at 120 fps for each height which was translated to lateral displacements on the x-y measuring plane. Fig. 5(a)

displays quadratic mean (RMS) of x/y oscillations recorded for each beam eight. We fitted quadratic models to both groups of data. It was observed that magnitude of oscillations along the x axis were 50% larger compared to the case of y axis.

This oscillation was expected to affect larger beams on their first normal mode of oscillation. We can derive a theoretical upper bound to the height of a plastic beam being fabricated using this process with this conservative assumption, since we might expect that larger (first mode) oscillations to induce a large moment in the beam supporting base.

Following this line of thought we applied the Euler-Bernoulli [38] Eqs. (13) and (14) for the torsion moment ( $M$ ) and maximum deflection ( $c_h$ ) obtained at a given height ( $h$ ) using the y-direction RMS oscillation model. We estimated the maximum moment that the PLA beam resisted at the embedment from a cantilever beam flexion model [39] (worst case scenario). The inertia ( $I$ ) was obtained from the beam transversal section using a Young modulus ( $E$ ) and fatigue stress ( $S_f$ ) of PLA. From these models we derived a maximum printable height of 658 cm which yields a manufacturing volume of 5922 cm<sup>3</sup>.

$$M = \frac{S_f c_h}{I} \tag{13}$$

$$c_h = \frac{h^2 M}{3EI} \tag{14}$$

Table 4 shows the dimensions, volume, building dimensions, height rate and volume rate of some popular 3D printers compared to estimations of the capability of the Koala 3D. Koala 3D is able to manufacture a column 12 times higher than itself while printing with PLA, before the structure fails due to oscillation. The column height will be

Table 4  
Machine and part dimensions of Koala 3D compared to popular desktop 3D printers.

| 3D Printer                         | Machine Dimensions (cm <sup>3</sup> ) | Part Dimensions (cm <sup>3</sup> ) | Height Ratio                 | Volume Ratio |
|------------------------------------|---------------------------------------|------------------------------------|------------------------------|--------------|
| Makerbot                           | 52.8 × 44.1 × 41                      | 28.5 × 19.5 × 16.5                 | 0.4                          | 0.1          |
| Formlab                            | 35 × 33 × 52                          | 14.5 × 14.5 × 17.5                 | 0.3                          | 0.06         |
| Blackbelt                          | 400 × 450 × 800                       | 340 × 340 × 1300                   | 1.6                          | 1            |
| Koala 3D (using PLA)               | 24 × 15 × 53                          | 3 × 3 × 658                        | 12.4                         | 0.3          |
| Koala 3D (using stronger material) | 24 × 15 × 53                          | Limited by material strength       | Limited by material strength | > 1          |

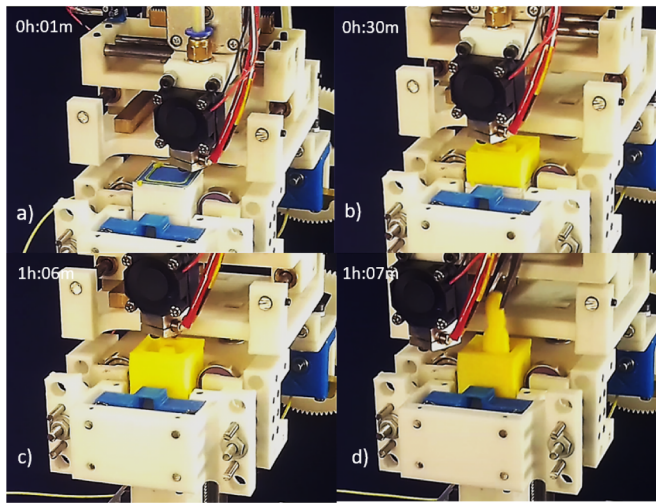


**Fig. 6.** Time frames of the manufacturing process of an object with complex morphology (a moai) in the center of a column. (a) The process begins with the extruder printing the column contour; (b) The column and the object are simultaneously manufactured during the printing process; (c) The process ends with the printing of its center (d) The object is extracted using needle-nose pliers.

limited by the strength of the printed material but not restricted to the printing process used by Koala.

## 5.2. Free-form fabrication

We explored the printer's capability to produce objects of an arbitrary shape inside the printed column. Fig. 6 displays time frames required in fabricating a moai statue (See supporting video 2). The figure was selected for its oblong shape. The statue was produced inside the  $30 \times 30$  cm column and taken outside the printing area using calipers. The printing process lasted one hour.

## 5.3. Energy distribution

Koala 3D's energy consumption was determined while printing a  $10 \times 10 \times 10$  mm PLA cube. We monitored the electric consumption of the printer's head heater, stepper motors, and carriage mechanisms independently using ACS712 Hall effect linear current sensors. The

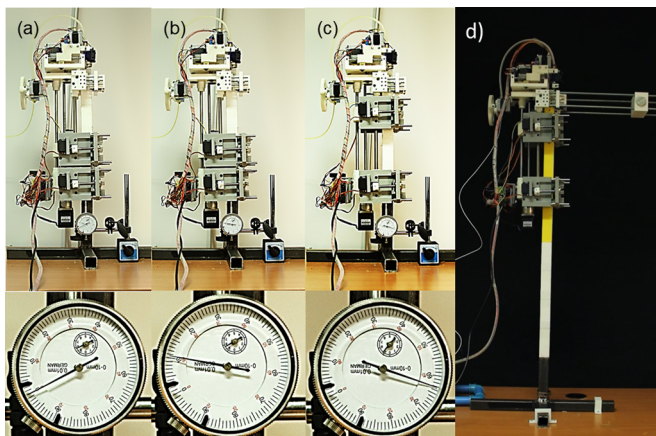


**Fig. 7.** (a–c) Examples of using a micrometer to measure machine drop during reanchoring. The machine is initially suspended by the CCC. Subsequently, (a) The LCC engages and CCC disengages. (b) Subsequent motion of the CCC results in an increased drop. (d) An example of producing a large beam. Supporting video 2 shows the machine in action while printing this beam.

maximum power consumption reached 50 W during a normal operation. A total of 36 kJ was required to print the cube of which 53% was used for nozzle heating, 41% in motor motion, and only 6% was in clamping operations performed by the servo motors.

## 5.4. Surface quality and shape preservation

We measured the resulting surface quality of five samples printed with Koala 3D. Samples were  $30 \times 30 \times 60$  mm rectangular columns with a  $20 \times 20 \times 60$  mm hollow core. The printing speeds and layer heights were chosen from values that are normally used for the extruder diameter (E3D volcano extruder [32] with a nozzle of 0.4 mm diameter). High-resolution images from the surface of the samples were acquired using an Olympus BH microscope (Olympus <https://www.olympus-lifescience.com>). Table 5 displays arithmetic rugosity of the surface profile with pictures for different combinations of layer height and printing speed. A layer height of 0.2 mm and printing speed of 50 mm/s lead to the smallest arithmetic rugosity (sample 2). Choosing a smaller layer height (sample 1) resulted in more fluctuations over the surface and coarser rugosity.

We compared the results of producing a more complex part with Koala 3D versus other FDM 3D printers to assess the structural preservation and esthetic performance. Table 6 shows the planar (x/y) and vertical (z) maximum deviation measured in millimeters while printing the resultant part shown in Table 6. Compared to Replicator 2, Koala 3D displays a slightly coarser performance on the plane but a better performance on the vertical axis. Ultimaker 2 performs better on the horizontal and vertical axes. We can conclude that the esthetic performance, accuracy, and capability qualification of Koala 3D is average compared to most popular 3D printers.

## 6. Discussion

The demonstrated free form fabrication capabilities of the machine imply that complex, intricate structures can be produced inside beams. Alternatively, the auxiliary navigation walls (outer squared structure) can be removed after fabrication. As Fig. 8(b) suggests, variations of the printer might produce much wider objects, that can overcome volumetric restrictions imposed by most 3D printers. However, this is not the primary intention of the proposed concept.

The proposed printing scheme can be applied to any domain that requires a complex part with high aspect ratio. This includes potential aerospace applications and construction tasks that use columns with intricate varying internal structure. Examples include the construction of terrestrial or extra-terrestrial non-regular antennae or complex truss-based solar arrays and deployments. Bio-inspired and artistic columns, aircraft wings, wind turbine blades, helix spiral turbine blades and a variety of other helix structures also demand parts with high aspect ratio.






The current demonstration opens many avenues for future research and applications in construction and product development industries. Other potential avenues for further development include exploring the use of the current 3D printing process on collaborative construction tasks. Fig. 8(c) illustrates this concept by showing two Koala 3D printers fabricating a truss structure (a chair). This will require developing the additional capability of autonomously traversing across the joints of the structure. These capabilities have already been introduced in the context of structure reconfiguring robots developed by Li et al. [40] and Yoon et al. [41]. Interestingly, these robots are similar in size to the Koala 3D Printer.

## 7. Conclusion

We have presented Koala 3D, the first climbing 3D printer that can navigate vertically along the same structure being produced by itself. In contrast to other processes, our machine does not resort to external

**Table 5**

Arithmetic rugosity obtained for common layer heights and printing speeds used to print with a nozzle extruder with a 0.4 mm diameter. The profile shown is in the z-direction of printing. The second sample shows the best performance with low rugosity and good esthetic performance.

| Sample | Layer height (mm) | Printing speed (mm/s) | Arithmetic rugosity ( $\mu\text{m}$ ) | Profile picture  |
|--------|-------------------|-----------------------|---------------------------------------|--|
| 1      | 0.1               | 50                    | 23.76                                 |  |
| 2      | 0.2               | 50                    | 16.57                                 |  |
| 3      | 0.3               | 50                    | 30.2                                  |  |
| 4      | 0.3               | 150                   | 38.09                                 |  |
| 5      | 0.3               | 20                    | 29.91                                 |  |

arms, auxiliary gantry, rails, or scaffolding. Therefore, the construction is not limited by the size of these supplementary elements.

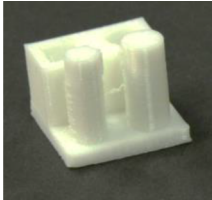
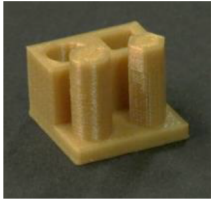
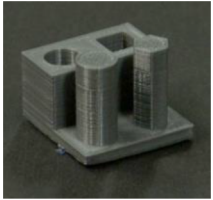
A broad range of experiments were conducted to characterize and understand the proposed concept. It was demonstrated that 3D printing is possible using the proposed printing-reanchoring-printing scheme. Experiments and performance evaluations were executed at the desktop scale with materials commonly used for 3D printing (PLA plastic). We identified a theoretical limit to the height of objects produced using these materials. It was caused by the reduced mechanical strength of PLA but not the fabrication process itself. The use of stronger materials will certainly serve to extend these limits.

We detected, characterized, and proposed solutions for three important problems in climbing 3D printers. The problems are (1) the machine drop after reanchoring, (2) the structural oscillation at high aspect ratios, and (3) the initial alignment between part and base. Addressing these problems will be important in developing autonomous machines that can climb along the same structures they produce.

In future work we plan to address some limitations of the current design. For example, the mechanism used for anchoring to a new point is complex and requires two servo motors on each clamping carriage. Another limitation is given by the extra weight used as counterweight. In future designs we expect to exploit the lessons from the current experience and produce a simple design that avoids the use of counterweight thanks to a more symmetric distribution of weight. We also expect to address the challenge of climbing with less actuators and less weight on the entire mechanism.

**Table 6**

Tolerance of a standard model for Koala 3D and other two printers.

|                    | Replicator 2  | Ultimaker 2  | Koala 3D  |
|--------------------|---|--|---|
| x/y tolerance (mm) | 0.4   | 0.2  | 0.5   |
| z tolerance (mm)   | 0.08  | 0.01   | 0.02  |
| Sample Picture     |  |  |  |

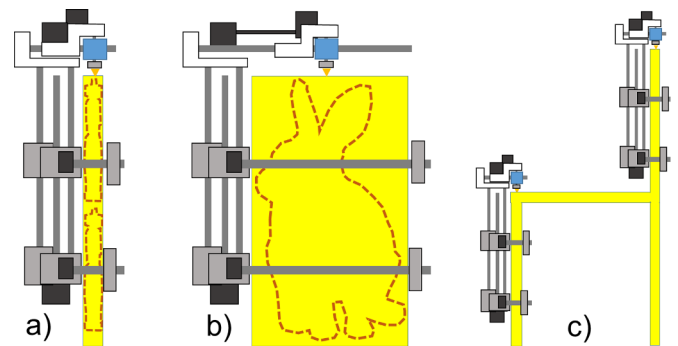


**Fig. 8.** Some variations of the printing concept discussed in this paper. (a) Current implementation. (b) Illustration of how the current concept can be extended to a much wider setting. (c) A more distant derivation of the current concept for producing structures with a team of collaborating printers. This requires incorporating the capability of printers to traverse the truss structure joints.

**CRediT authorship contribution statement**

**Maximiliano Vélez:** Methodology, Software, Validation, Investigation, Visualization. **Efrén Toala:** Software, Data curation. **Juan Cristóbal Zagal:** Conceptualization, Methodology, Formal analysis, Investigation, Resources, Writing - review & editing, Visualization, Supervision, Funding acquisition.



## Declaration of Competing Interest

None.

## Supplementary materials

Supplementary material associated with this article can be found, in the online version, at doi:10.1016/j.rcim.2020.101950.

## References

- [1] K. Kolarevic, *Architectural in the Digital Age: Design and Manufacturing*, Spon Press, New York, 2003.
- [2] E. Malone, H. Lipson, Fab@Home: the personal desktop fabricator kit, *Rapid Prototyp. J* 13 (2007) 245–255.
- [3] A. Calderon, J. Griffin, J.C. Zagal, BeamMaker: an open hardware high-resolution digital fabricator for the masses, *Rapid Prototyp. J* 20 (3) (2014) 245–255.
- [4] R. Jones, P. Haufe, E. Sells, P. Irvani, V. Oliver, C. Palmer, A. Bowyer, RepRap – The replicating rapid prototyper, *Robotica* 29 (2011) 177–191.
- [5] H. Lipson, M. Kurman, *Fabricated: The New World of 3D Printing*, John Wiley & Sons, Indianapolis, 2013, pp. 7–20.
- [6] D. Mourtzis, M. Doukas, F. Psarommatas, A multi-criteria evaluation of centralized and decentralized production networks in a highly customer-driven environment, *CIRP Ann. Manufact. Technol.* 61 (2012) 427–430.
- [7] L. Bo-hu, L. Zhang, W. Shi-long, T. Fei, C. Jun-wei, J. Xiao-dan, S. Xiao, C. Xu-dong, Cloud manufacturing: a new service-oriented networked manufacturing model, *Comput. Integrat. Manufact. Syst.* 16 (1) (2010) 1–7.
- [8] H. Nyman, P. Sarlin, From bits to atoms: 3D printing in the context of supply chain strategies, *Proceedings of the Hawaii Conference on System Sciences, IEEE*, 2014, pp. 4190–4199.
- [9] C. Mota, The rise of personal fabrication, *Proceedings of the 8th ACM Conference on Creativity and Cognition*, 2011, pp. 279–288.
- [10] T.D. Ngo, A. Kashani, G. Imbalzano, K.T. Nguyen, D Hui, Additive manufacturing (3D printing): a review of materials, methods, applications and challenges, *Compos. Part B: Eng.* 143 (2018) 172–196.
- [11] Y. Yang, X. Song, X. Li, Z. Chen, C. Zhou, Q. Zhou, Y. Chen, Recent progress in biomimetic additive manufacturing technology: from materials to functional structures, *Adv. Mater.* 30 (36) (2018) 1706539(2018).
- [12] U. Jammalamadaka, K. Tappa, Recent advances in biomaterials for 3D printing and tissue engineering, *J. Funct. Biomater* 9 (1) (2018) 22.
- [13] P. Urhal, A. Weightman, C. Diver, P. Bartolo, Robot assisted additive manufacturing: a review, *Robot Comput. Integr. Manuf.* 59 (2019) 335–345.
- [14] J. Jiang, X. Xu, J. Stringer, Optimization of process planning for reducing material waste in extrusion based additive manufacturing, *Robot Comput. Integr. Manuf.* 59 (2019) 317–325.
- [15] J. Jiang, J. Stringer, X. Xu, R.Y. Zhong, Investigation of printable threshold overhang angle in extrusion-based additive manufacturing for reducing support waste, *Int. J. Comput. Integr. Manufact.* 31 (10) (2018) 961–969.
- [16] S. Keating, N. Oxman, Compound fabrication: a multi-functional robotic platform for digital design and fabrication, *Robot Comput. Integr. Manuf.* 29 (6) (2013) 439–448.
- [17] R.P. Hoyt, J. Cushing, J. Slostad, G. Jimmerson, Trusselator: on-orbit fabrication of high-performance composite truss structures, *Proceedings of the AIAA SPACE 2014 Conference and Exposition*, 2014, p. 4337.
- [18] B. Levedahl, R.P. Hoyt, T. Silagy, J. Gorges, N. Britton, J. Slostad, Trusselator™ technology for in-situ fabrication of solar array support structures, *Proceedings of the AIAA Spacecraft Structures Conference*, 2018, p. 2203.
- [19] S. Keating, J. Leland, L. Cai, N. Oxman, Toward site-specific and self-sufficient robotic fabrication on architectural scales, *Sci. Robot.* 2 (5) (2017) 1–15.
- [20] X. Zhang, L. Mingyang, J. Hui Lim, Y. Weng, Y. Wei, D. Tay, H. Pham, Q.-C. Pham, Large-scale 3D printing by a team of mobile robots, *Automat. Construct.* 95 (2018) 98–106.
- [21] Minibuilders by Iaac, Small robots printing big structures. <http://robots.iaac.net/>, (accessed October 10, 2019).
- [22] M. Kayser, L. Cai, S. Falcone, C. Bader, N. Inglessis, B. Darweesh, N. Oxman, FIBERBOTS: an autonomous swarm-based robotic system for digital fabrication of fiber-based composites, *Construct. Robot.* 2 (1–4) (2018) 67–79.
- [23] BlackBelt. <https://blackbelt-3dcom/>, (accessed October 20, 2019).
- [24] G. Hunt, F. Mitzalis, T. Alhinai, 3D printing with flying robots, *Proceedings of the IEEE Hong Kong Conference on Robotics and Automation (ICRA)*, 2014, pp. 4493–4499.
- [25] J. Werfel, K. Petersen, R. Nagpal, Designing collective behavior in a termite-inspired robot construction team, *Science* 343 (2014) 754–758.
- [26] E. Bonadeau, M. Dorigo, G. Theraulaz, Inspiration for optimization from social insect behaviour, *Nature* 405 (2000) 39–42.
- [27] J. Willmann, F. Augugliaro, T. Cadalbert, R. D'Andrea, F. Gramazio, M. Kohler, Aerial robotic construction towards a new field of architectural research, *Int. J. Architect. Comput.* 10 (3) (2012) 439–459.
- [28] A. Mirjan, F. Augugliaro, R. D'Andrea, F. Gramazio, M. Kohler, Building a bridge with flying robots, *Proceedings of the Robotic Fabrication in Architecture, Art and Design*, 2016, pp. 34–47.
- [29] E.M. Golafshani, S. Talatahari, Predicting the climbing rate of slip formwork systems using linear biogeography-based programming, *Appl. Soft Comput.* 70 (2018) 263–278.
- [30] Makerbot Replicator. <https://www.makerbot.com/>, (accessed August 15 2019).
- [31] Ultimaker. <https://ultimaker.com/>, (accessed August 15 2019).
- [32] J-Head Extruder. [https://reprap.org/wiki/J\\_Head\\_Nozzle](https://reprap.org/wiki/J_Head_Nozzle), (accessed November 10 2019).
- [33] J. Griffey, The types of 3D printing, *Libr. Technol. Rep.* 50 (5) (2014) 8–12.
- [34] R. Budynas, J. Nisbett, Power transmission case study, *Shigley's Mechanical Engineering Design*, McGraw-Hill Companies, New York, 2011, pp. 933–951.
- [35] Designfax. <http://www.designfax.net/cms/dfx/opens/article-view-dfx.php?nid=4&bid=373&et=featurearticle&pn=01>, (accessed: October 10 2019).
- [36] E. Gustafsson, Investigation of friction between plastic parts, master's thesis, chalmers university of technology, Gothenburg (2013).
- [37] Optitrack. <http://optitrack.com/>, (accessed: October 20 2019).
- [38] O. Bauchau, J. Craig, Euler-Bernoulli beam theory, *Structural Analysis*, Springer Nature, Atlanta, 2009, pp. 173–221.
- [39] B.M. Tymrak, M. Kreiger, J.M. Pearce, Mechanical properties of components fabricated with open-source 3-D printers under realistic environmental conditions, *Mater Des.* 58 (2014) 242–246.
- [40] F. Nigl, S. Li, J.E. Blum, H. Lipson, Structure-reconfiguring robots: autonomous truss reconfiguration and manipulation, *IEEE Robot. Automat. Mag.* 20 (3) (2013) 60–71.
- [41] Y. Yoon, D. Rus, Shady 3D: a robot that climbs 3D trusses, *Proceedings of the Conference on Robotics and Automation, IEEE*, 2007, pp. 4071–4076.